International Journal of Engineering Trends and Technology
ISSN: 2231-5381/ https://doi.org/10.14445/22315381/IJETT-V74I4P126

Volume 74 Issue 4, 342-359, April 2026

Original Article

Tone Aware Convolutional Neural Network with Conditional Feature Pyramid Network for Skin Cancer Classification

Priyadarshini Mayigowda[1], Zafar Ali Khan N[2]

[1,2]*School of Computer Science and Engineering, Presidency University, Bangalore, India*

[1]*Corresponding Author : zafaralikhan@presidencyuniversity.in*

Received: 08 January 2026 Revised: 20 February 2026 Accepted: 20 February 2026 Published: 29 April 2026

Abstract *- Skin cancer classification involves identifying and categorizing skin lesions as either malignant or benign, depending on visual appearance, which helps doctors detect and monitor skin cancer more effectively. However, classifying the severity of skin cancer from dermoscopic images is difficult due to subtle and overlapping visual features, which leads to inconsistencies and enhances misclassification. This research proposes a Tone Aware Convolutional Neural Network with Conditional Feature Pyramid Network (TACNN-CFPN) to classify skin cancer accurately. In TACNN, CFPN is incorporated, which enables the model to adaptively perform specified feature extraction paths based on skin tone, become more sensitive to the visual characteristics of each skin tone, and lead to more accurate identification of lesions. TACNN adapts feature learning to the specific skin tone of input, which addresses visual variations in lesion appearance and enhances classification accuracy across diverse populations. Resizing ensures uniform image dimension, whereas over- and undersampling methods balance class distribution that minimizes bias and enhances model generalization. Therefore, the TACNN-CFPN achieves better accuracy of* 98.84%, 99.84%, 98.87%, and 98.53% *on the ISIC-2019, ISIC-2020, HAM10000, and PAU-UFES-20 datasets compared to existing methods, namely Deep CNN.*

Keywords *- Conditional Feature Pyramid Network, Tone Aware Convolutional Neural Network, Resizing, Skin Cancer, Undersampling.*

1. Introduction

Skin cancer is a widespread condition that arises from abnormal skin cell growth because of excessive exposure to ultraviolet radiation. It is distinguished by abnormal cell growth in the skin, which leads to the formation of a tumor [1]. Skin cancer is categorized as melanoma and non-melanoma, where non-melanoma [2] involves squamous cell and basal cell carcinoma. Melanoma [3] is regarded as the deadliest form of skin cancer and is growing rapidly all over the world. Typically, skin cancer screening is performed by clinicians via visual examination, which is error-prone. Dermoscopy, a noninvasive imaging method, enhances lesion visibility by eliminating surface reflection and capturing magnified and well-illuminated skin images. Dermatologists employ the ABCD [4] rule, which determines Asymmetry, Border irregularity, Color variation [5], and Diameter to evaluate suspicious pigmented lesions [6]. Apart from dermoscopy [7], the visual examination, and biopsy [8] are used to identify skin cancer; however, these two are not considered in this research due to their subjective variability and invasive nature. A dermoscopic approach employs a dermoscopy device to acquire more detailed lesion images on the skin surface [9]. Melanoma accounts for nearly 55,000 deaths all over the world each year. Despite the high fatality rate, melanoma has a 5-year survival rate of across 93% when it is identified early [10]. Different methods have been used for the automatic detection of melanoma skin cancer [11]. Presently, Artificial Intelligence (AI) is used to help physicians and dermatologists more effectively, which leads to high accuracy and reliability in diagnosis [12].

In AI, Machine Learning (ML) [13] methods are utilized to categorize classes for developing diagnostic tools [14, 15]. However, achieving high diagnostic performance is challenging because the ML model needs hand-crafted features, and dermoscopic images often exhibit low inter-class differences and high intra-class variations. Moreover, conventional approaches such as Support Vector Machine (SVM) and k-nearest neighbors based on predefined features struggle to encapsulate the intricate and variable nature of medical imaging data [16]. Hence, Deep Learning (DL) methods like Convolutional Neural Network [17, 18], Vision Transformer [19], and so on are used extensively in the diagnosis and classification of skin cancers [20]. These

methods automatically learn to extract features from the previous stage, which enables high accuracy in skin cancer detection and classification.

1.1. Problem Statement and Objective

Skin cancer classification includes categorizing skin lesions into different types depending on visual and structural features. However, classifying the severity of skin cancer from dermoscopic images is difficult due to subtle and overlapping visual features, which lead to inconsistencies and misclassification. To address this gap, a novel Tone Aware Convolutional Neural Network with Conditional Feature Pyramid Network (TACNN-CFPN) is proposed by determining the skin tone utilizing Individual Typology Angle (ITA) and Fitzpatrick, and activating corresponding CFPN branches. This ensures a model for extracting tone-specific multi-scale features and enhances lesion representation by minimizing irrelevant background. Hence, the proposed TACNN-CFPN achieves more accurate differentiation between malignant and benign lesions that minimizes misclassification.

1.2. Contribution

- ITA and Fitzpatrick are used to differentiate between light and dark skin more accurately from dermoscopic images. This tone-aware estimation minimizes bias, improves lesion representation, and enhances the robustness of skin cancer classification.
- CNN automatically learns discriminative features, namely shape, texture, and color variations, from dermoscopic images. This eliminates dependence on handcrafted features and enhances accurate differentiation between malignant and benign skin lesions.
- CFPN is incorporated to address the variations in lesion appearance across different skin tones. By using CFPN, the network dynamically adapts the multi-scale features extracted depending on skin tone, resulting in more precise performance on specific-tone lesion patterns.

This research paper is organized as follows: Section 2 provides a detailed literature survey. Section 3 explains the proposed methodology, and Section 4 evaluates the experimental results. The conclusion of this research is given in Section 5.

2. Literature Survey

Skin cancer classification involves identifying benign and malignant skin lesions using dermoscopic images, which are crucial for accurate diagnosis and effective treatment. Existing methods are analyzed and reviewed in this section with findings, benefits, and limitations. Essam H. Houssein et al. [21] established a Deep Convolutional Neural Network (DCNN) for classifying skin cancer lesions. In image intensity, the model becomes less sensitive to variation by normalizing pixel values, which results in more consistent and reliable performance across different medical images. Moreover, all images were reshaped to a standardized size that not only reduces consistency in image dimension but also memory utilization and computational effectiveness. Finally, DCNN was used to classify skin cancer due to automatically extracting and learning intricate features from dermoscopic images. Nevertheless, DCNN struggled with overfitting due to imbalanced data, which poorly generalizes to new or unseen images.

Zhanlin Ji et al. [22] presented an Enhanced Feature Fusion and Attention Mechanism (EFFAM-Net) to classify multi-class skin lesions. Initially, Attention Residual Learning ConvNeXt (ARLC) was utilized for extracting low-level features such as textures and colors in images. Later, the deep-layer network block was replaced with the Parallel ConvNeXt (PCNXt) block, which allows for capturing richer and more intricate features. The Multi-Scale Efficient Attention Feature Fusion (MEAFF) block was utilized to enhance feature extraction at different scales, which enables the model to effectively capture more comprehensive features. However, attention modules lead to suboptimal feature prioritization in noisy or low-quality images, which results in inaccurate attention weight allocation.

Yousef S. Alsahaf et al. [23] developed a Residual Deep CNN (RDCNN) to classify skin lesions. Instead of using filters that slide along with the horizontal axis, numerous convolution filters were utilized to perform multi-layer feature extraction. The developed method addresses the class imbalance issue by converting the dataset from image-label pairs into a combination of image data and a corresponding weight vector. Nevertheless, RDCNN suffered from gradient vanishing in deep architectures, which leads to instability during training.

Sasmita Padhy et al. [24] introduced a hybrid DL called Residual Network-Long Short-Term Memory (R-LSTM50) to classify skin lesions. The data augmentation was employed to solve the scarcity of data for specific classes that impact the classification model. The R-LSTM50 employed ResNet-50 to extract spatial features, whereas the LSTM layer captures temporal modeling performance. However, integrating spatial and temporal features causes difficulties in effectively capturing static skin lesion patterns, which minimizes classification accuracy.

V. S. S. Bala Tripura Sathvika et al. [25] suggested two pipelines using Support Vector Machine (SVM) and AlexNet for skin lesion classification. Initially, skin lesion images were preprocessed, and later, skin regions were segmented. The lesion regions were subdivided into four regions depending on the function of intensity mapping. The bisectional features were extracted from subdivided regions, and the extracted features were trained by the SVM method. Nevertheless, SVM struggled with high-dimensional features from AlexNet, which caused scalability and performance issues on large skin

lesions. Sara Medhat et al. [26] developed an Iterative Magnitude Pruning (IMP)-based AlexNet to classify skin cancer. While IMP was applied to AlexNet, memory usage and running time were decreased without a significant loss in accuracy. IMP was a pruning neural network that assigned scores to network connections depending on the absolute value that corresponds to the relational effect on trained network accuracy. However, IMP-based AlexNet lost significant features during pruning that minimize classification accuracy on complex skin cancer images.

Amany M. Sarhan et al. [27] presented a CNN model to enhance classification accuracy. The presented method employed various CNN models, namely DenseNet201, XceptionNet, MobileNetV2, DenseNet121, and GoogleNet, to classify skin cancer. Data augmentation and transfer learning methods were incorporated to refine model performance. Moreover, hyperparameter tuning was performed by utilizing Ant Colony Optimization (ACO).

Omneya Attallah et al. [28] suggested a Scaling to classify skin cancer by leveraging a multi-directional compact CNN ensemble and Gabor Wavelet (GW). Scaling obtains a wide range of image information through splitting images into multiple directional sub-bands by utilizing GW. Also, SCaLiNG integrates attributes taken from CNN with actual images and sub-bands obtained from GW. Scaling employs minimum Redundancy Maximum Relevance (mRMR) to select the most appropriate features.

Geunho Jung et al. [29] introduced an automated image-based technique to map the skin tone using optical methods and DL. The method produces skin tone maps by utilizing the illuminant spectrum, then segments the skin region from face images, and determines the corresponding skin tone map. The introduced method was analyzed by generating skin tone maps over three standard illuminants: D45, D65, and D85. From the overall analysis, existing methods exhibit clear research gaps, such as class imbalance, inability to capture subtle and overlapping features, poor generalization, and skin tones, which minimize model performance. To address this issue, TACNN-CFPN is proposed to classify skin cancer accurately. TACNN captures subtle and overlapping lesion features by incorporating skin tone information, whereas CFPN captures contextual information. This process enhances generalization, minimizes bias, and obtains better performance, which leads to more reliable skin cancer classification.

3. Proposed Methodology

This research proposes TACNN-CFPN to classify skin lesions accurately. Initially, HAM10000, ISIC-2019, ISIC-2020, and PAD-UFES-20 are used to determine model performance. The obtained images are preprocessed using resizing and random over- and undersampling. Later, ITA and Fitzpatrick are used to estimate the skin tone effectively. At last, the proposed TACNN-CFPN is applied to classify skin lesions. Figure 1 demonstrates a workflow diagram of the proposed method.

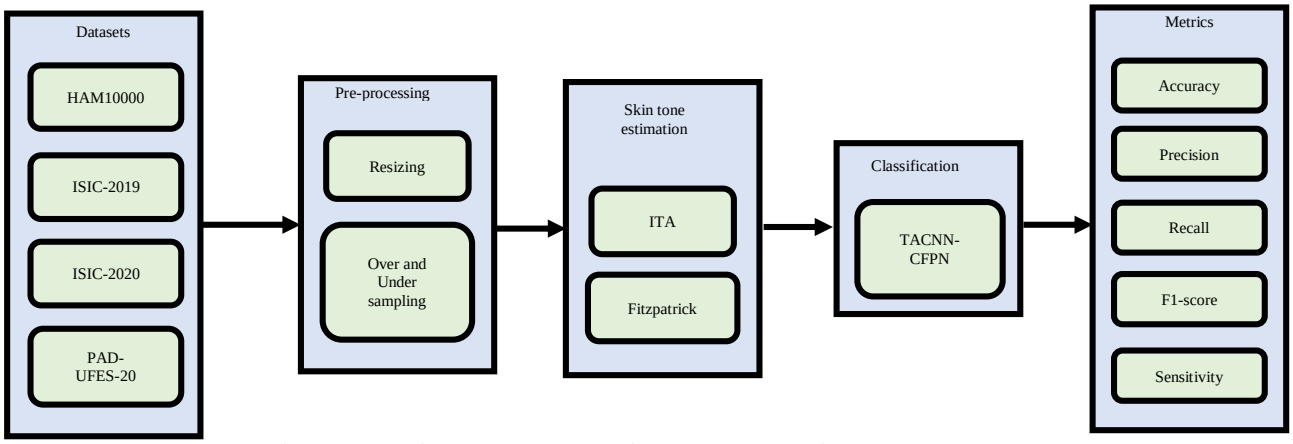

Fig. 1 Workflow diagram of the proposed method for skin cancer classification using dermoscopy images

3.1. Datasets

This research employs four publicly available datasets called HAM10000 [30], ISIC-2019 [31], ISIC-2020 [32], and PAD-UFES-20 [33] to determine model performance. Each dataset has a diverse collection of dermoscopic images and associated metadata. A detailed description of these datasets is provided below. HAM10000: It has 10,015 dermoscopy images with skin lesions, and these skin lesions are classified into seven different classes depending on characteristics. It contains high-quality images with both malignant and benign instances. Each image is accompanied by metadata such as patient age, lesion type, clinical information, and anatomical region. Figure 2 demonstrates sample images from HAM10000. ISIC-2019: It is a collection of dermoscopic images from the International Skin Imaging Collaboration (ISIC) with nine different classes to classify skin lesions. It involves 25,331 images associated with a particular diagnostic category, indicating the type of skin lesion present. Figure 3 represents sample images from the ISIC-2019.

Fig. 2 Representative samples of dermoscopic images from HAM10000, which indicate the types of diverse skin lesion classes

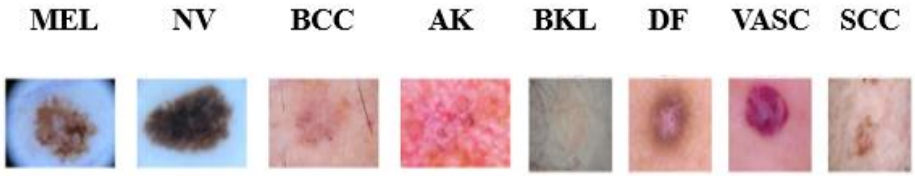

Fig. 3 Sample dermoscopic images from ISIC-2019, which represent different types of skin lesion classes

Fig. 4 Sample dermoscopic images from ISIC-2020, which demonstrate different types of skin lesion classes

Fig. 5 Representative dermoscopic sample images from the PAD-UFES-20 dataset

ISIC-2020: It has 33,126 dermoscopic images with benign and malignant from over 2000 patients. All images are related to people with unique patient IDs, which ensures accurate mapping between images and patient data. Figure 4 demonstrates sample images from ISIC-2020.

PAD-UFES-20: It involves 1,373 patients, 1,641 skin lesions, and presents 2,298 images. Every image is associated with a skin lesion and a patient in the metadata. Figure 5 displays sample images from the PAD-UFES-20 datasets, and those images undergo preprocessing for further processing.

3.2. Preprocessing

The gathered images are preprocessed utilizing resizing, random oversampling, and undersampling to ensure uniformity in input size and balance class distribution. Image resizing ensures a consistent input size for the neural network, which provides efficient learning. Random oversampling solves class imbalance by duplicating minority class images, which prevents bias towards classes. The following information about these methods is outlined below in detail.

Resizing: The obtained images are resized to 224×224 to classify skin cancer to ensure uniformity in input size, which is essential for consistent training of the CNN model. This size is chosen due to a standard dimension that balances computational efficiency and retention of appropriate visual details. Unlike models that employ pre-trained weights, CNN is trained from scratch; hence, consistent input dimensions are significant to stabilize the learning process. Moreover, resizing avoids the distortion that arises from varied image sizes and maintains significant lesions.

Random over- and undersampling: It is used to address the class imbalance issue where malignant lesions are underrepresented. For the HAM10000, PAD-UFES-20, and ISIC-2019 datasets, the oversampling [34] method is applied due to the small number of images, which assists in augmenting minority classes and obtaining a balanced dataset without increasing complexity. For the ISIC-2020 dataset, both undersampling [35] and oversampling methods are used since the number of images is larger. This helps to avoid an overabundance of highly similar data, which balances the data effectively. Figures 6 to 9 depict learning instances of original vs. balanced class distribution for four publicly available datasets. Later, preprocessed images are passed through the classification process.

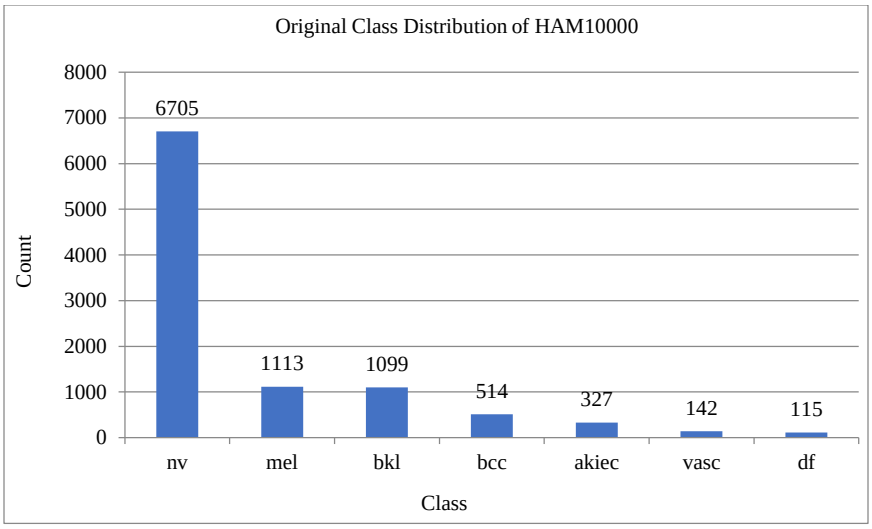

(a)

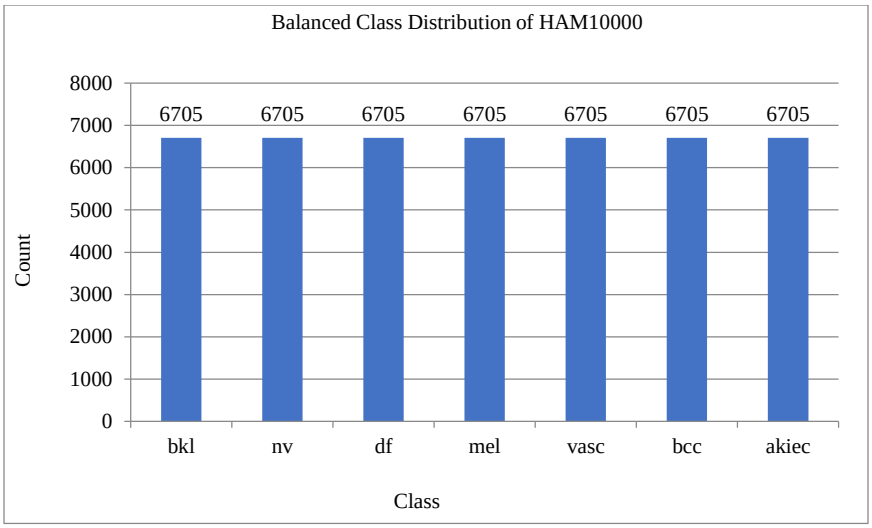

(b)

Fig. 6 Learning instances showing (a) original vs. (b) balanced class distribution for the HAM10000 dataset after the resampling process

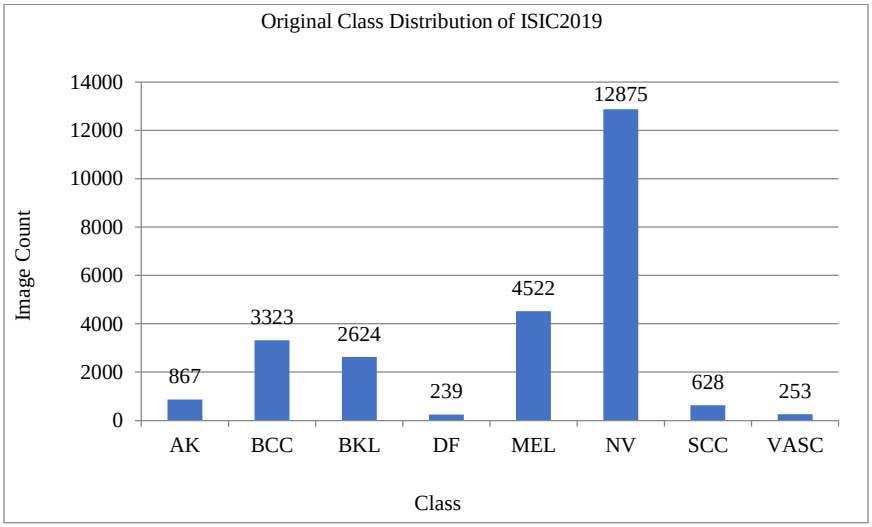

(a)

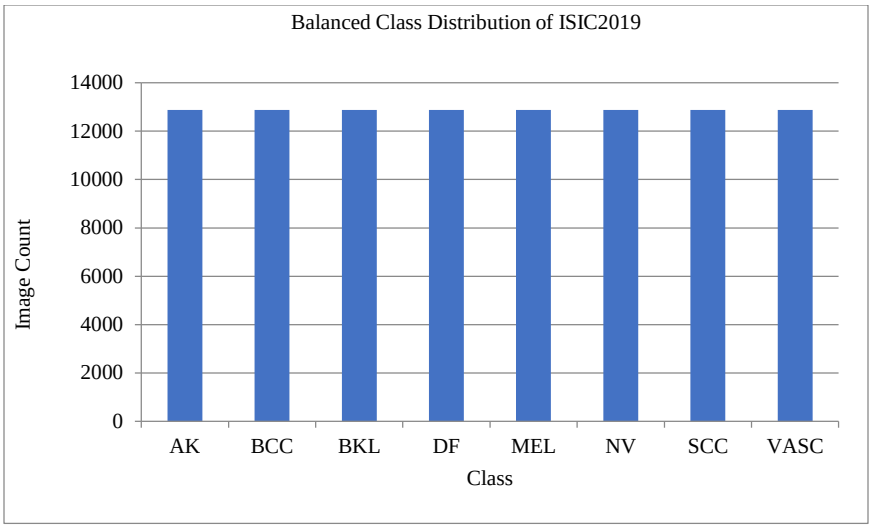

(b)

Fig. 7 Learning instances of (a) original vs. (b) balanced class distribution for the ISIC2019 after the resampling process

(a)

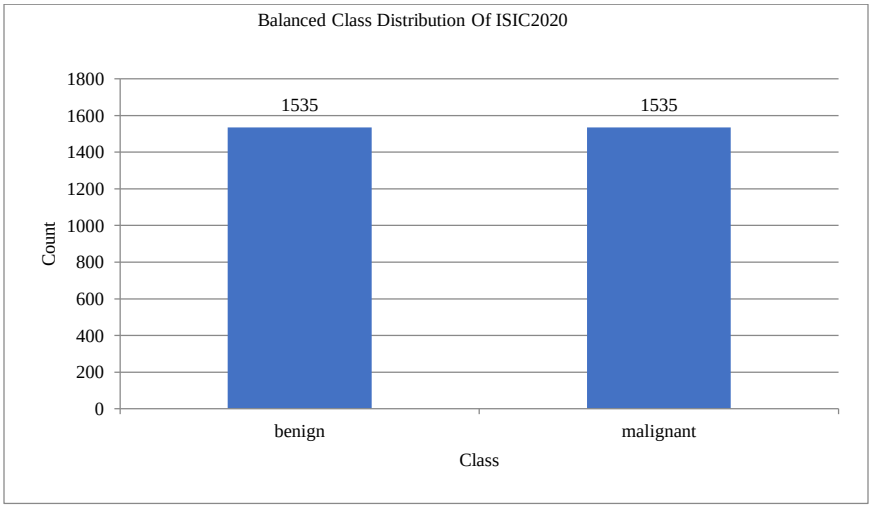

(b)

Fig. 8 Comparison of (a) original vs. (b) balanced class distribution for the ISIC2020 after the resampling process

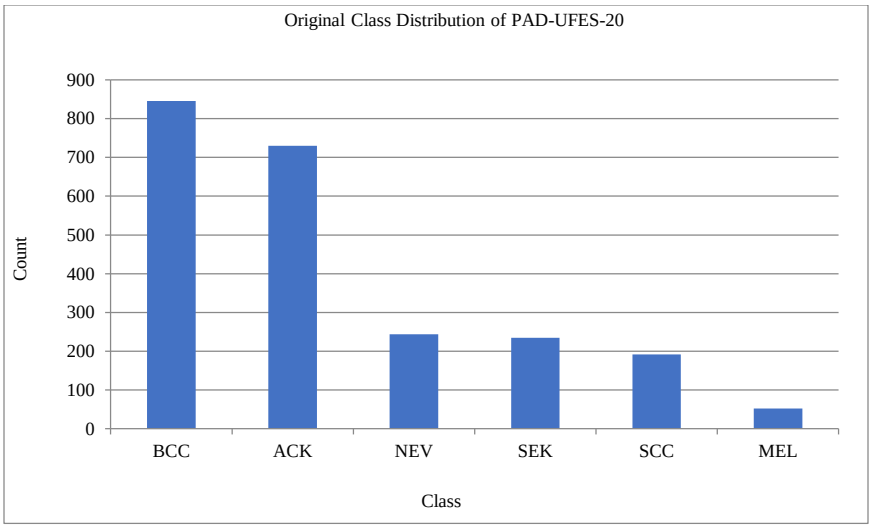

(a)

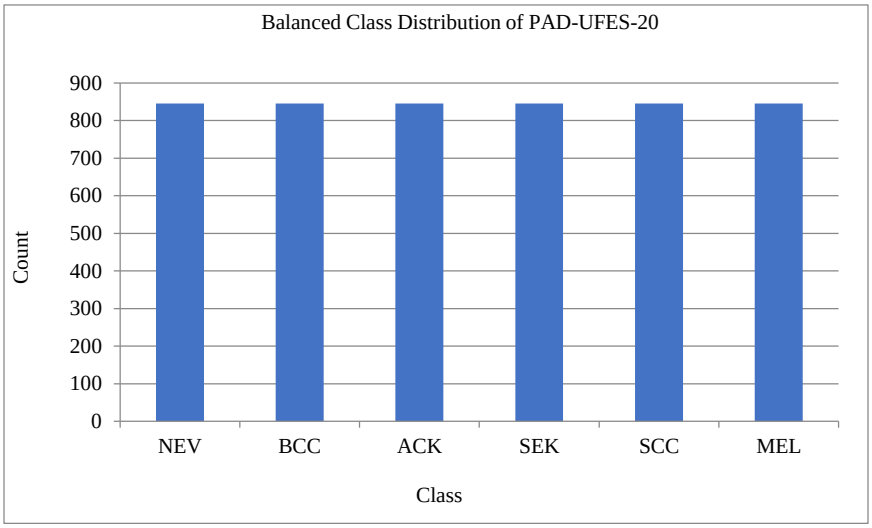

(b)

Fig. 9 Comparison of (a) original vs. (b) balanced class distribution for the PAD-UFES-20 after the resampling process

3.3. Skin Tone Estimation

The preprocessed images are fed as input to this stage to evaluate skin tone effectively. Since the dataset does not contain skin color information, Individual Typology Angle (ITA) and Fitzpatrick skin type are used to estimate the skin tone as dark or light skin.

This captures inherent pigmentation differences that influence lesion contrast and texture visibility in dermoscopic images. ITA determined using the CIELAB color space is chosen due to being less sensitive to illumination variations than Red Green Blue (RGB)-based methods, which ensures more reliable tone estimation.

The Fitzpatrick scale is split into six categories of skin types depending on Ultraviolet (UV) response, ranging from type 1 (fair skin that always burns and never tans) to type 6 (dark skin that never burns). Moreover, ITA offers a more objective, colorimetry-based measure to quantify skin's inherent pigmentation, where a higher ITA value represents lighter skin tones. ITA values are calculated from images using the CIELAB color space in Equation (1).

$$\mathrm{ITA}(\mathrm{L}\times,\mathrm{B}\times) = \arctan\left(\frac{\mathrm{L}\times-50}{\mathrm{b}}\right).\frac{180}{\pi} \quad (1)$$

Where $L\times$ and $B\times$ indicate lightness and blue-yellow opponents of the CIELAB color space. Estimated ITA from images is utilized as an indication of associated skin darkness.

For directly utilizing the Fitzpatrick type classifier to categorize subjects, a proxy value is introduced for skin darkness. Therefore, this process ensures robust performance for the relationship between skin color and quality. Later, the estimated skin color is passed through a classification process using the proposed TACNN-CFPN.

3.4. Classification

After estimating skin color, TACNN-CFPN is used to classify skin cancer accurately. Based on the estimated skin tone, the model enhances lesion representation, resulting in enhanced performance and greater fairness in classification. CNN [36] is particularly effective for skin cancer classification due to automatically learning hierarchical features from estimated skin tone. It leverages convolutional filters by capturing both low-level and high-level visual patterns, such as shape and texture, which are significant in distinguishing between benign and cancerous lesions. CNN's deep architecture allows it to capture intricate relationships from images, which enhances diagnostic accuracy.

Therefore, CNN learns robust and discriminative features, which makes it highly appropriate for skin cancer classification. In classical CNN, CFPN is incorporated to address the variation in lesion appearance across different skin tones. CNN extracts features uniformly, which leads to less accuracy on darker skin, where lesions often have lower contrast.

Unlike conventional multi-scale CNN and FPN, which employ uniform feature fusion irrespective of image characteristics, TACNN-CFPN introduces a conditional feature process that enables the network to learn tone-specific representation. This minimizes bias caused by heterogeneous skin tone distribution and enhances lesion feature discrimination. A detailed step-by-step process of TACNN-CFPN is explained below.

Convolutional layer: It automatically extracts meaningful features from input data by applying a set of filters. These filters identify significant patterns, namely textures, edges, and shapes, which are crucial for skin cancer. The primary concept of the convolution process between an input image I of dimension $m \times m$ and a filter F with dimension $n \times n$ is represented in Equation (2).

$$\mathrm{C} = \mathrm{I} \otimes \mathrm{F} \tag{2}$$

Where $\otimes$ indicates the convolution operation, and C represents a convolution map size. Typically, Rectified Linear Unit (ReLU) is used on the convolution map C to introduce nonlinearity into the network, enabling it to learn complex patterns using Equation (3).

$$\mathrm{C_a} = \mathrm{f(C)} \tag{3}$$

Where C_a demonstrates a convolution map after applying a nonlinear activation function f.

Pooling: It is employed to minimize the dimension. C_a, which minimizes network computational complexity. During the pooling process, the kernel K of size $(s_p \times s_p)$ is sliding across C_a, where s_p illustrates the number of patches. The mathematical formula for pooling is represented in Equation (4).

$$\mathrm{P} = \mathrm{Pool(C_a)} \tag{4}$$

Where P represents the pooling map, max-pooling is used to downsample feature maps that minimize spatial dimensions while retaining the most significant information. Selecting the maximum value within a defined window preserves strong activations that indicate prominent features in the image. This operation assists in enhancing computational efficiency and minimizing overfitting risk by introducing a more compact representation.

CFPN: It enables dynamic feature extraction based on input context, which enables the network to adaptively adjust multi-scale for varying characteristics by containing two parallel branch routes. The light skin branch is used to capture high contrast and fine-grained features presented in lighter skin tones. The dark skin branch is used to enhance edge preservation and subtle texture details, which are often less visible in darker skin tones. The model processes input features exclusively via the corresponding branch of FPN, which ensures that the network processes tone-relevant visual cues more effectively.

One of the route processes multi-scale features from bottom to top that connect high-level features with low resolution and high semantics, whereas low-level features have low semantics and high resolution. Another network route operates from top to bottom; after passing through numerous layers, rich semantic information from upper layers is progressively transferred to lower-layer features for fusion, and Figure 10 represents the structure of CPFN. In Figure 10, the bottom-up feature map sequence on the left is denoted as {C2, C3, C4, C5}, while the corresponding top-down feature pyramid structure on the right is represented as {P2, P3, P4, P5}. During the feature extraction process, the model employs a step size of {4, 8, 16, 32} for different levels of feature hierarchy. To construct the feature pyramid, each higher-level feature map is processed using a 1×1 convolution kernel with a stride of one. In the upsampling stage, feature maps are resized and aligned using 256 channels, which ensures a consistent representation of features across all levels. This is to ensure that its dimensions are matched with the lower feature map for effective fusion. Later, a 3×3 convolution is applied to remove aliasing artifacts introduced during the 2-fold upsampling process to acquire a feature map.

Fully Connected (FC): It is used to integrate the features learned from previous layers and make final classification decisions. It connects each neuron to all activations in the previous layer, which enables the network to combine learned features for accurate output performance.

The hyperparameter is chosen based on a grid search to ensure optimal performance. A learning rate of 0.001 is selected to provide stable convergence, whereas the Adam optimizer adapts learning ability. ReLU activation is used to solve the vanishing gradient issue, which provides rapid training, and the categorical cross-entropy loss function measures class probability differences, which makes it suitable for multi-class skin cancer classification. Algorithm 1 represents the pseudo-code of the proposed method to ensure reproducibility.

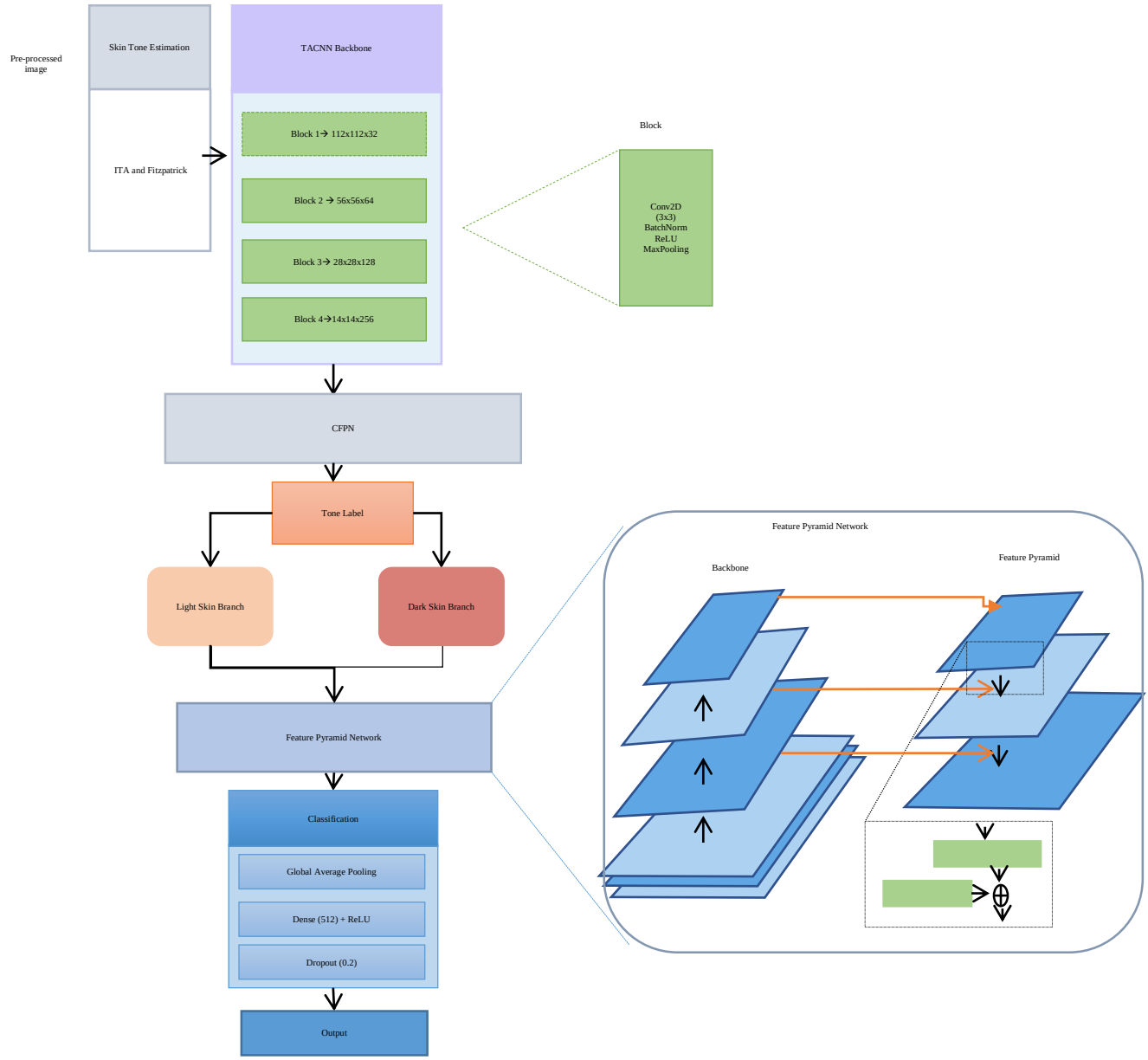

Fig. 10 Architecture of TACNN-CPFN for skin lesion classification from dermoscopic image

Algorithm 1 of the proposed TACNN-CFPN

Input: Datasets D= {ISIC-2019, ISIC-2020, HAM1000, PAU-UFES-20}

Output: Predicted skin lesion class

Start

Step 1: Datasets and Preprocessing

i) Load datasets D.

ii) Split datasets into 80% training and 20% testing.

iii) For each image I in D do

a) Resize I into a uniform dimension 224 × 224.

b) Apply random over-sampling and under-sampling to balance the classes.

End For

Step 2: Skin Tone Estimation
For each image *I*, do
a) Convert RGB into CIELAB.
b) Calculate ITA using Equation (1).
c) Assign Fitzpatrick type
If ITA> threshold then
Tone← Light
Else
Tone ←Dark
End If
End For

Step 3: Classification using TACNN-CFPN
For each image *I*, do
a) Extract hierarchical features using CNN.
b) Obtain feature maps C2, C3, C4, and C5.
End For
Construct a top-down FPN.
P5←Conv 1×1 (C5)
P4←Up (P5) + Conv 1×1 (C4)
P3←Up (P4) + Conv 1×1 (C3)
P2←Up (P3) + Conv 1×1 (C2)
If Tone==Light, then
Employ the Light-FPN branch.
Else
Apply the Dark-FPN branch.
End If
Fuse P2, P3, P4, P5
Apply global average pooling.
Feed features into FC layers.
Apply a softmax classifier.
Return predicted lesion class.

End

4. Experimental Results

A TACNN-CFPN is simulated by employing a Python 3 environment with the Windows 10 operating system, 64 GB Random Access Memory (RAM), and an Intel i7 processor, respectively. Accuracy, F1-score, recall, and precision are used to assess model performance, which are shown in the following Equations (5) to (8).

$$\text{Accuracy} = \frac{\text{TP+TN}}{\text{TP+TN+FP+FN}} \tag{5}$$

$$\text{Recall} = \frac{\text{TP}}{\text{TP+FN}} \tag{6}$$

$$\text{F1} - \text{Score} = \frac{2\text{TP}}{2\text{TP+FP+FN}} \tag{7}$$

$$\text{Precision} = \frac{\text{TP}}{\text{TP+FP}} \tag{8}$$

Where FP indicates false positive, TN determines true negative, FN represents false negative, and TP illustrates true positive.

4.1. Performance Analysis

Table 1 demonstrates the performance analysis of different classifiers. Compared to existing methods, namely CNN, DCNN, TACNN, CNN-CFPN, ViT-CFPN, and Swin transformer-CFPN, the proposed TACNN-CFPN achieves a high accuracy of 98.84%, 99.84%, 98.87%, and 98.53% on ISIC-2019, ISIC-2020, HAM10000, and PAU-UFES-20 datasets due to its adaptation to different skin tones that directly solves visual inconsistency. By employing Fitzpatrick, the model determines the skin tone of each input image and selectively activates FPN branches for light and dark skin.

Table 1. Performance analysis of different classifiers for an accurate diagnostic process using skin cancer datasets

Methods	Datasets	Accuracy (%)	Specificity (%)	Precision (%)	AUC (%)	Recall (%)	F1 Score (%)
CNN	ISIC-2019	89.78±1.05	90.13±1.56	89.34±0.85	90.87±0.72	89.51±0.71	89.42±0.83
	ISIC-2020	91.42±0.85	91.34±1.02	90.79±0.74	91.92±0.65	91.03±0.65	90.9±0.74
	HAM1000	90.03±0.74	90.66±0.86	89.67±0.63	91.47±0.60	89.94±0.56	89.8±0.69
	PAU-UFES-20	89.66±0.71	90.1±0.72	89.08±0.60	90.84±0.54	88.94±0.47	89.01±0.64
DCNN	ISIC-2019	96.78±0.65	97.92±0.64	96.22±0.52	98.76±0.41	96.90±0.36	96.56±0.59
	ISIC-2020	97.12±0.42	97.50±0.61	96.85±0.46	98.04±0.35	96.40±0.32	96.62±0.51
	HAM1000	95.67±0.36	96.30±0.54	94.80±0.42	97.15±0.30	95.20±0.28	94.99±0.43
	PAU-UFES-20	95.02±0.31	95.95±0.52	94.11±0.35	96.78±0.26	94.80±0.22	94.45±0.38
TACNN	ISIC-2019	97.44±0.21	97.99±0.46	96.85±0.25	98.4±0.22	96.78±0.15	96.81±0.31
	ISIC-2020	97.80±0.18	97.90±0.41	97.35±0.15	98.55±0.18	97.20±0.11	97.27±0.28
	HAM1000	96.50±0.14	96.80±0.35	95.90±0.11	97.45±0.14	96.00±0.10	95.95±0.21
	PAU-UFES-20	96.12±0.10	96.64±0.28	95.43±0.08	97.22±0.09	95.82±0.09	95.61±0.14
CNN-CFPN	ISIC-2019	97.96±0.18	98.21±0.33	97.74±0.19	98.87±0.15	97.69±0.12	97.88±0.24
	ISIC-2020	98.12±0.16	98.36±0.29	98.05±0.14	99.04±0.13	98.01±0.10	98.17±0.22
	HAM1000	97.21±0.13	97.54±0.27	97.03±0.12	98.11±0.11	97.06±0.09	97.14±0.19
	PAU-UFES-20	96.78±0.11	97.22±0.24	96.51±0.09	97.84±0.10	96.64±0.08	96.73±0.17

ViT-CFPN	ISIC-2019	98.32±0.14	98.57±0.26	98.19±0.16	99.12±0.11	98.2± 0.10	98.35±0.18
	ISIC-2020	98.74±0.12	98.9± 0.23	98.61±0.13	99.38±0.09	98.66±0.08	98.72±0.16
	HAM1000	97.86±0.11	98.11±0.21	97.74±0.10	98.94±0.08	97.79±0.09	97.83±0.15
	PAU-UFES-20	97.41±0.10	97.88±0.19	97.05±0.08	98.46±0.07	97.16±0.08	97.22±0.14
Swin transformer-CFPN	ISIC-2019	98.61±0.10	98.74±0.21	98.53±0.12	99.38±0.08	98.55±0.09	98.66±0.14
	ISIC-2020	99.12±0.08	99.24±0.19	99.06±0.11	99.5± 0.06	99.08±0.07	99.15±0.12
	HAM1000	98.33±0.09	98.51±0.18	98.29±0.10	99.36±0.07	98.34±0.08	98.42±0.13
	PAU-UFES-20	98.02±0.08	98.44±0.17	97.91±0.09	99.12±0.06	97.95±0.07	98.07±0.12
TACNN-CFPN	ISIC-2019	98.84±0.06	98.83±0.07	98.84±0.06	99.65±0.04	98.83±0.05	98.83±0.06
	ISIC-2020	99.84±0.04	99.84±0.05	99.84±0.08	99.84±0.03	99.84±0.07	99.84±0.08
	HAM1000	98.87±0.05	98.88±0.03	98.87±0.04	99.92±0.01	98.88±0.04	98.85±0.04
	PAU-UFES-20	98.53±0.03	99.70±0.02	98.53±0.03	99.98±0.06	98.52±0.03	98.52±0.06

This enables the network to better enhance appropriate features depending on tone-specific characteristics. Hence, TACNN-CFPN obtains superior performance compared to existing methods. Table 2 indicates performance analysis of computational time complexity based on training time, memory usage, and inference time. The proposed TACNN-CFPN maintains low computational complexity by reusing a shared backbone at the FPN stage. Instead of training separate methods for different skin tones, CFPN integrates both tone branches in a single network that minimizes model redundancy. Therefore, this method results in less memory usage and rapid convergence without affecting classification accuracy. The p-value from the paired t-test based on accuracy is utilized to determine whether the performance difference between the two methods is statistically significant and not due to random variation. The experiments are conducted over five independent runs by utilizing five different random seeds across identical dataset splits. The null hypothesis H0 assumes that there is no statistically significant difference between the existing and proposed methods, whereas the alternative hypothesis H1 considers the significant enhancement obtained by the proposed method.

Table 2. Computational time complexity and statistical analysis of the proposed TACNN-CFPN in terms of training time, memory usage, inference time, and p-value from paired t-test

Datasets	Training time (s)	Memory usage (MB)	Inference time (s)	p-value from paired t-test
ISIC-2019	6.12	2856	1.07	0.041
ISIC-2020	2.24	1783	0.42	0.022
HAM1000	4.01	2141	0.59	0.036
PAU-UFES-20	1.53	1448	0.33	0.038

Figure 11 depicts the performance evaluation of epoch vs. accuracy for the proposed TACNN-CFPN across 50 epochs: a) HAM10000, b) ISIC-2019, c) ISIC-2020, and d) PAU-UFES-20 datasets.

In each graph, training accuracy increases steadily and converges above 0.9, which reflects effective learning from the dataset. The validation accuracy represents a steady rise that nearly follows the training curve with slight fluctuations.

In validation accuracy, these small drops represent certain variations in generalization performance. Consequently, the convergence of both metrics represents a fitted model with less overfitting. Such consistent patterns across all graphs demonstrate reliable validation and training accuracy.

Figure 12 illustrates the performance analysis of Epoch vs. Loss for a) HAM10000, b) ISIC-2019, c) ISIC-2020, and d) PAU-UFES-20 datasets. During the initial stage, the model quickly adapts to data, reflected by a rapid decrease in loss. During training, training loss remains slightly lower than validation loss, which demonstrates that the model is generalizing effectively. Such observations support the robustness and reliability of the model in managing skin cancer classification tasks.

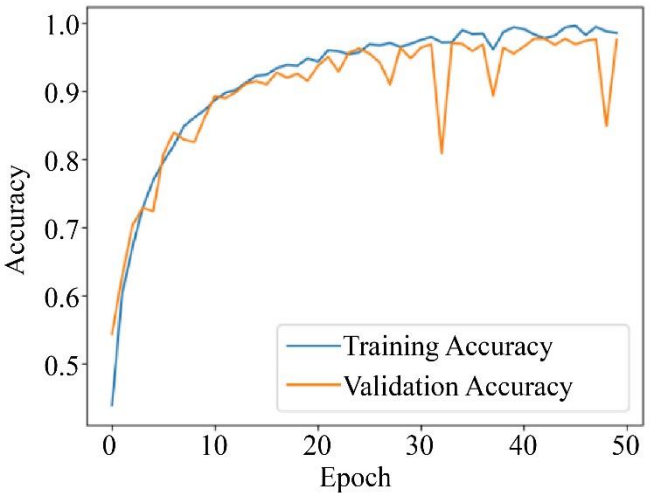

(a)

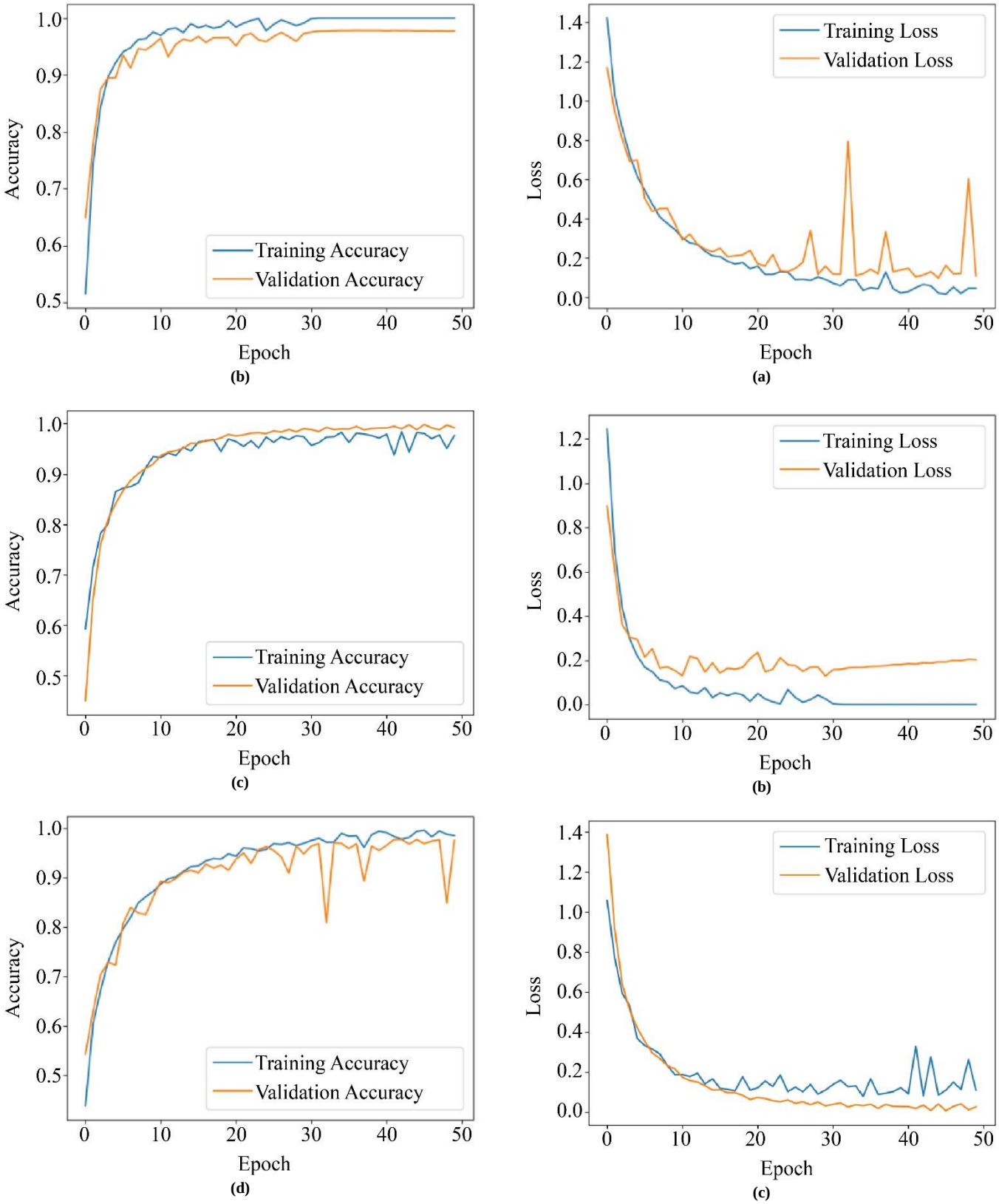

Fig. 11 Analysis of Epoch vs. Accuracy for four available datasets: (a) HAM10000, (b) ISIC-2019, (c) ISIC-2020, (d) PAU-UFES-20

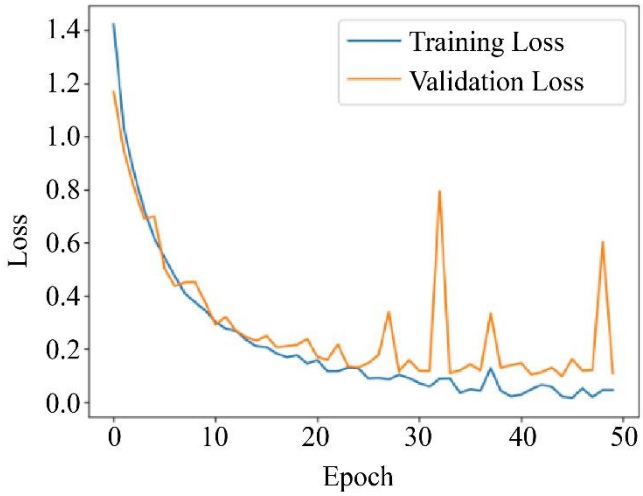

(d)

Fig. 12 Analysis of Epoch vs. Loss for different datasets: (a) HAM10000, (b) ISIC-2019, (c) ISIC-2020, (d) PAU-UFES-20

Figure 13 represents a confusion matrix for the classification model across multiple classes. In the HAM10000 and PAU-UFES-20 datasets, high classification accuracy is obtained with minimal misclassifications.

In ISIC-2019, the model depicts robust multiclass performance with diagonal dominance via minor misclassification.

In ISIC-2020, only one misclassification occurred, which highlights the model's strong diagnostic reliability. A highly consistent value with diagonals across all confusion matrices highlights a well-generalized and accurate model.

These results demonstrate that the proposed method is highly efficient for both binary and multiclass skin lesion classification.

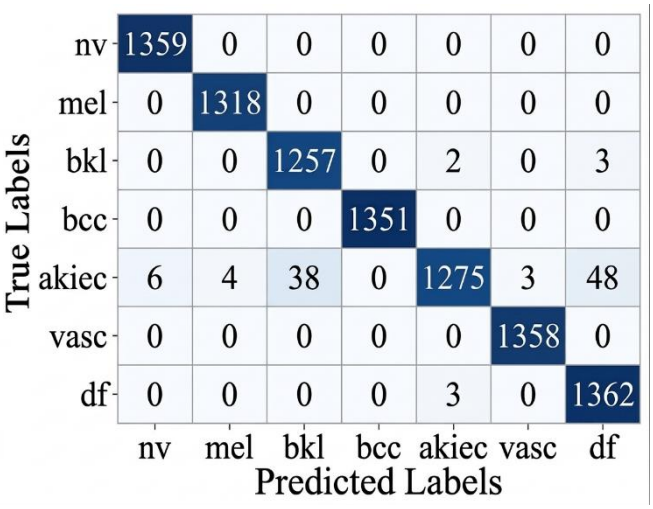

(a)

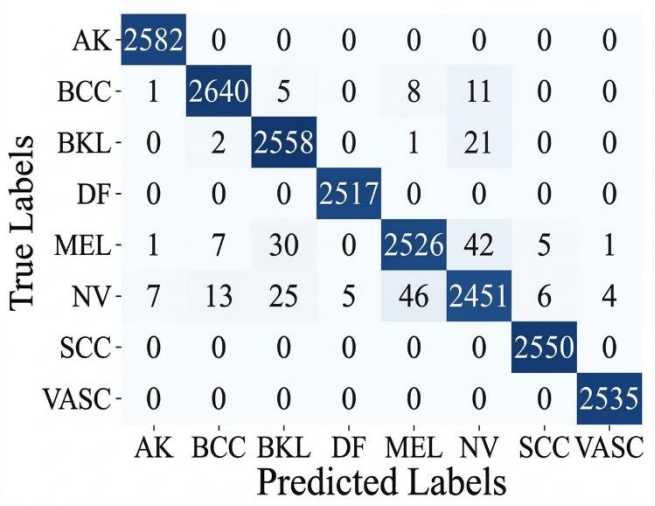

(b)

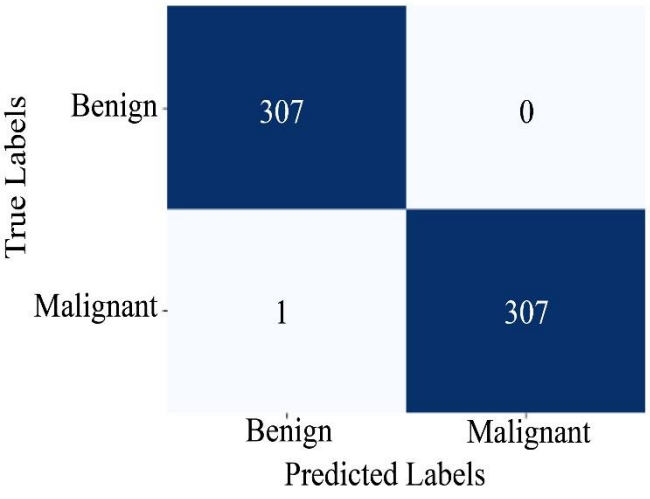

(c)

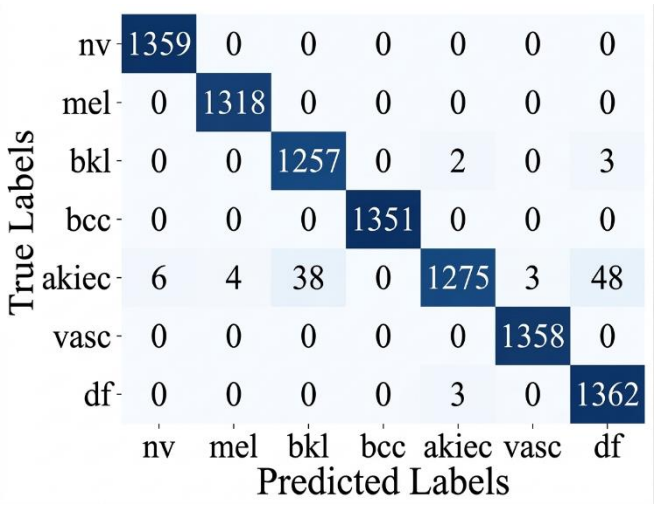

(d)

Fig. 13 Performance evaluation of confusion matrix, which represents the classification performance: (a) HAM10000, (b) ISIC-2019, (c) ISIC-2020, (d) PAU-UFES-20

Figure 14 demonstrates the analysis of the Area Under the Curve (AUC) for different datasets.

In all graphs, curves lie near the top-left corner, which illustrates a high True Positive Rate (TPR) and low False Positive Rate (FPR).

Most of the classes attain an AUC of nearly 1.0000, which exhibits a better classification process.

In the ISIC-2020 dataset, binary classification indicates that benign and malignant classes obtain AUCs of 1.000 and 0.9968.

These outcomes show the model's robustness in distinguishing subtle differences in dermoscopic images with high reliability.

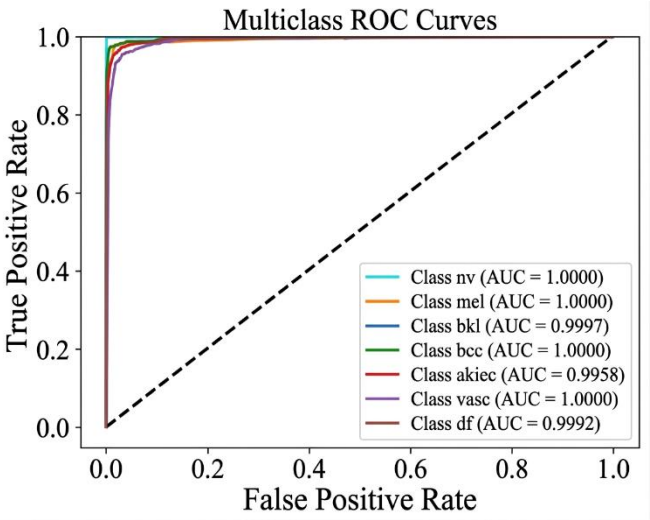

(a)

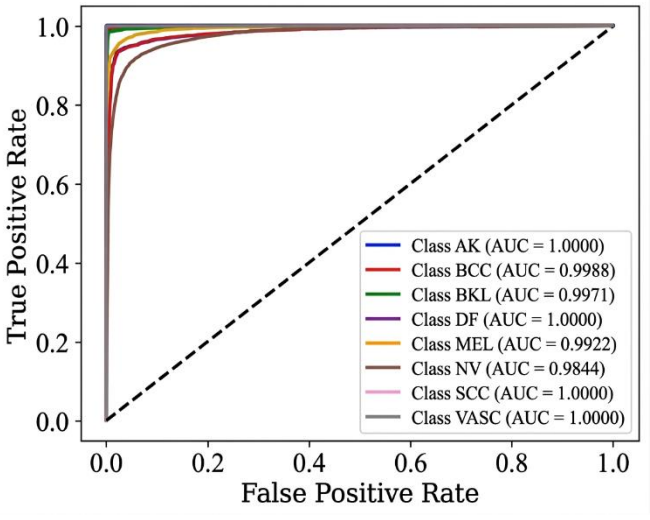

(b)

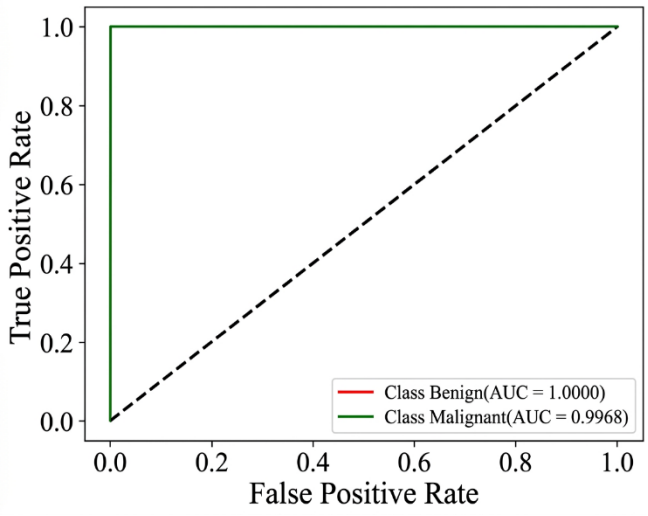

(c)

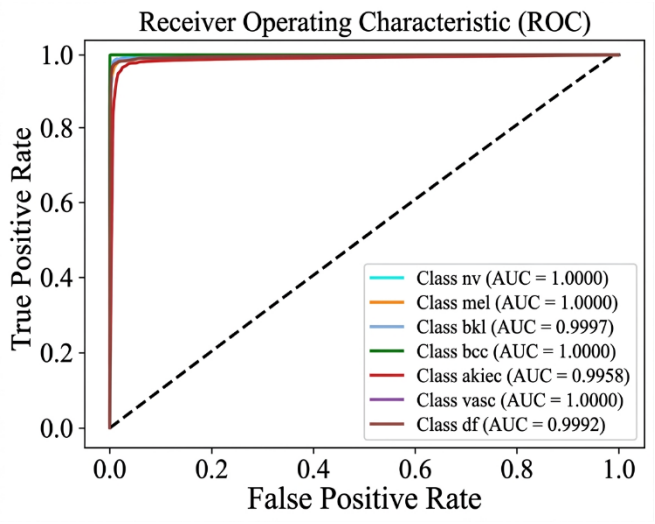

(d)

Fig. 14 Performance evaluation of AUC, which displays discriminative performance of the proposed method on different datasets across skin lesions: (a) HAM10000, (b) ISIC-2019, (c) ISIC-2020, (d) PAU-UFES-20

4.2. Generalization Analysis

Figure 15 demonstrates performance analysis for different classifiers on the dog-skin disease. To analyze generalization, an additional dataset called "dog skin disease" is evaluated, which contains images of canine skin conditions.

By analyzing another dataset, the proposed method obtains high accuracy, which shows superior generalization ability.

This outcome proves that the model's performance is not limited to the primary dataset but adapts effectively to distant data distributions.

This provides flexibility and robustness of the model in managing new or unseen data effectively.

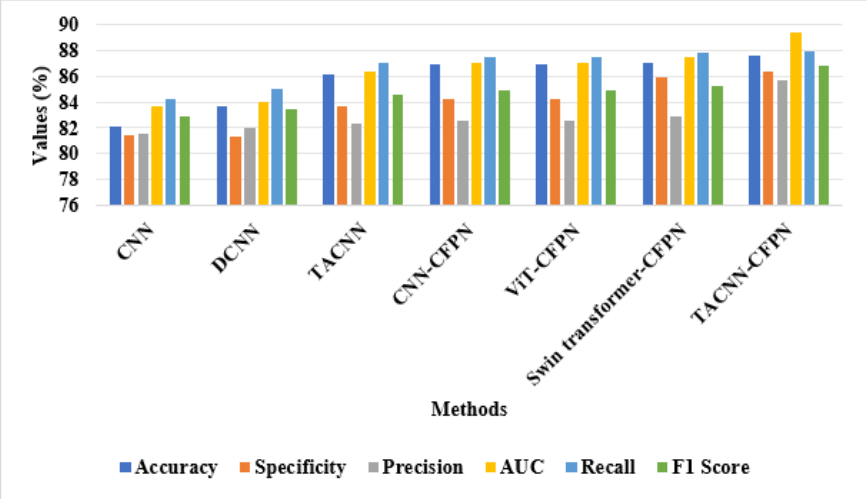

Fig. 15 Graphical representation of different classifiers on the dog-skin disease dataset to assess generalization ability

4.3. Ablation Study

Table 3 provides an ablation study for TACNN-CFPN. The proposed method obtains higher accuracy than standard CNN and CNN+FPN due to explicitly accounting for variation in lesion appearance over different skin tones. While classical CNN and FPN extract features uniformly, the tone-aware model adjusts extraction based on Fitzpatrick skin type, which enables it to capture tone-specific lesion characteristics better. Therefore, the proposed method obtains superior classification performance on underrepresented skin tone groups compared to other combination methods for different datasets.

Table 3. Ablation study analyzing the impact of the proposed TACNN-CFPN components on classification performance over different datasets

Methods	Dataset	Accuracy (%)	Specificity (%)	Precision (%)	AUC (%)	Recall (%)	F1 Score (%)
CNN	ISIC-2019	97.68	97.72	97.55	98.9	97.60	97.57
	ISIC-2020	98.6	98.60	98.42	99.2	98.51	98.45
	HAM1000	97.12	97.2	96.90	98.5	97.00	96.95
	PAU-UFES-20	96.75	97.10	96.60	98.00	96.70	96.65
CNN+FPN	ISIC-2019	98.25	98.3	98.2	98.25	98.22	98.21
	ISIC-2020	99.21	99.2	99.15	99.21	99.18	99.16
	HAM1000	98.12	98.15	98.05	98.11	98.08	98.06
	PAU-UFES-20	97.85	98.00	97.8	97.85	97.82	97.81
TACNN-CFPN	ISIC-2019	98.84	98.83	98.84	99.65	98.83	98.83
	ISIC-2020	99.84	99.84	99.84	99.84	99.84	99.84
	HAM1000	98.87	98.88	98.87	99.92	98.88	98.85
	PAU-UFES-20	98.53	99.70	98.53	99.98	98.52	98.52

4.4. Comparative Analysis

Table 4 demonstrates a comparative analysis of existing techniques on four publicly available datasets. Compared to existing methods such as [21-26], TACNN-CFPN achieves a better accuracy of 98.84%, 99.84%, 98.87%, and 98.53% on ISIC-2019, ISIC-2020, HAM10000, and PAU-UFES-20 datasets due to adapting the feature extraction process depending on the estimated skin tone of each input image. By separately using CFPN branches for dark and light skin, the model learns tone-specific patterns that enhance lesion representation. Therefore, the proposed method achieves a more reliable and accurate performance across a diverse population.

Table 4. Comparative analysis of the existing methods with the proposed method for skin cancer classification

Methods	Datasets	Precision (%)	Accuracy (%)	Recall (%)	Specificity (%)	F1 Score (%)
DCNN [21]	ISIC-2019	97.09	97.11	97.12	99.61	97.08
	HAM10000	98.56	98.50	98.51	99.73	98.48
EFAM-Net [22]	ISIC-2019	88.27	92.30	88.86	98.59	88.52

	HAM1000	90.23	93.95	91.44	98.44	90.78
RDNN [23]	ISIC-2019	72.56	94.65	70.78	96.78	71.33
	ISIC-2020	96.57	99.05	96.57	99.42	96.57
R-LSTM50 [24]	ISIC-2020	N/A	95.72	92.08	95.72	92.78
	HAM1000	N/A	94.23	92.41	90.33	93.46
AlexNet pipeline 2 [25]	HAM1000	N/A	98.66	95.82	96.58	95.96
	PAU-UFES-20	N/A	98.10	95.54	95.68	94.52
IMP AlexNet [26]	PAU-UFES-20	95.61	97.62	91.82	94.41	93.59
Xception [27]	HAM10000	97.0	96.5	97.0	N/A	97.0
GW+MobileNet+ShuffleNet+ ResNet-18+mRMR+Quadratic SVM [28]	HAM10000	91.70	91.70	91.70	N/A	91.70
Proposed TACNN-CFPN	ISIC-2019	98.84	98.83	98.83	98.83	98.83
	ISIC-2020	99.84	99.84	99.84	99.84	99.84
	HAM1000	98.87	98.86	98.88	98.88	98.85
	PAU-UFES-20	98.53	98.52	98.52	99.70	98.52

4.5. Discussion

The proposed TACNN-CFPN achieves better performance compared to existing methods due to the integration of skin tone within the feature extraction process. Unlike multi-scale CNN and FPN-based techniques that employ uniform feature aggregation, the proposed method adapts feature representation depending on estimated skin tone using ITA and Fitzpatrick. This ensures a model for capturing high-contrast lesion structure and edge patterns in darker skin tones that minimizes tone-induced bias representation. Also, CFPN improves multi-scale contextual learning by focusing on tone-relevant features. Hence, the proposed method obtains better classification accuracy of 98.84%, 99.84%, 98.87%, and 98.53% on different datasets and statistically significant performance. Unlike existing bias mitigation methods that focus on dataset balancing, the proposed TACNN-CFPN integrates skin tone awareness into the feature extraction process. By estimating skin tone utilizing ITA and Fitzpatrick, the network adapts tone-specific CFPN branches. This differs from conventional multi-scale CNN and FPN-based methods, which perform uniform feature aggregation without considering visual tone variations. The conditional mechanism enables the proposed TACNN-CFPN to capture high-contrast lesion patterns in lighter skin tones while preserving subtle texture and edge information in darker skin tones that minimize tone-induced representation bias.

Skin tone influences visual contrast, texture visibility, and color distribution in dermoscopic images that affect feature learning in CNN. The representation of conditioning multi-scale features on estimated skin tone enables the network to display tone-relevant discriminative information. This enhances more balanced representation learning and minimizes bias across skin tone subgroups. The proposed TACNN-CFPN is deployed as a decision-support module within an existing dermoscopic-based CAD system. Since lesion classification and skin tone estimation are established in a single forward pass, the framework does not need changes to the clinical acquisition workflow. The modular design enables integration with the hospital Picture Archiving and Communication System (PACS). Scalability is attained by CNN and CFPN that adapt tone-specific branches without increasing model parameters. This minimizes memory usage and supports efficient inference, which makes it suitable for benchmarking datasets.

5. Conclusion

This research proposes the TACNN-CFPN to accurately classify skin cancer. The integration of CFPN makes adaptive feature extraction based on specific skin tones for varying characteristics by containing two parallel branch routes. The light skin branch is used to capture high contrast and fine-grained features presented in lighter skin tones. The dark skin tones are used to enhance edge preservation and subtle texture details, which are often less visible in darker skin tones. This dynamic adaptation increases the model's sensitivity to specific tone lesion patterns that significantly enhance classification accuracy. Resizing ensures uniform input dimensions, whereas oversampling and undersampling solve the class imbalance issue, which enhances generalization.

The experimental outcomes illustrate that TACNN-CFPN obtains superior accuracy of 98.84%, 99.84%, 98.87%, and 98.53% on the ISIC-2019, ISIC-2020, HAM10000, and PAU-UFES-20 datasets compared to existing methods such as DCNN. The ablation study confirms that the effectiveness of TACNN-CFPN outperforms standard CNN and CNN+FPN variants. Moreover, the proposed method attains less computational complexity, which ensures efficiency. Although ITA determined that in CIELAB space minimizes sensitivity to illumination, variations in lighting conditions, imaging devices, and acquisition protocols still affect accuracy, as such variations change captured color and intensity values that directly influence computed components. Future research will explore clinically annotated skin tone labels, advanced illumination normalization techniques, and

multi-center clinical evaluations. Also, real-world data will be considered to validate the proposed method under practical deployment settings.

Conflicts of Interest

The author(s) declare(s) that there is no conflict of interest regarding the publication of this paper.

Funding Statement

Not applicable.

Acknowledgments

Authors 1 and Author 2 contributed equally to this work.

References

[1] Mawaddah Harahap et al., "Skin Cancer Classification using EfficientNet Architecture," *Bulletin of Electrical Engineering and Informatics*, vol. 13, no. 4, pp. 2716-2728, 2024. [CrossRef] [Google Scholar] [Publisher Link]

[2] Neven Saleh, Mohammed A. Hassan, and Ahmed M. Salaheldin, "Skin Cancer Classification based on an Optimized Convolutional Neural Network and Multicriteria Decision-Making," *Scientific Reports*, vol. 14, no. 1, pp. 1-19, 2024. [CrossRef] [Google Scholar] [Publisher Link]

[3] Usha Thirugnanam, and Nalini Joseph, "Skin Cancer Classification using Premature Convergence Strategy-based Artificial Jelly Search Optimization with Convolutional Neural Network," *International Journal of Intelligent Engineering & Systems*, vol. 17, no. 5, pp. 848-858, 2024. [CrossRef] [Google Scholar] [Publisher Link]

[4] Galib Muhammad Shahriar Himel et al., "Skin Cancer Segmentation and Classification using Vision Transformer for Automatic Analysis in Dermatoscopy-based Noninvasive Digital System," *International Journal of Biomedical Imaging*, vol. 2024, pp. 1-18, 2024. [CrossRef] [Google Scholar] [Publisher Link]

[5] Günay İlker, and İnik Özkan, "SADASNet: A Selective and Adaptive Deep Architecture Search Network with Hyperparameter Optimization for Robust Skin Cancer Classification," *Diagnostics*, vol. 15, no. 5, pp. 1-28, 2025. [CrossRef] [Google Scholar] [Publisher Link]

[6] Ali Atshan Abdulredah et al., "Towards Unbiased Skin Cancer Classification using Deep Feature Fusion," *BMC Medical Informatics and Decision Making*, vol. 25, no. 1, pp. 1-22, 2025. [CrossRef] [Google Scholar] [Publisher Link]

[7] Sara M.M. Abohashish, Hanan H. Amin, and E.I. Elsedimy, "Enhanced Melanoma and Non-Melanoma Skin Cancer Classification using a Hybrid LSTM-CNN Model," *Scientific Reports*, vol. 15, no. 1, pp. 1-23, 2025. [CrossRef] [Google Scholar] [Publisher Link]

[8] J.D. Dorathi Jayaseeli et al., "An Intelligent Framework for Skin Cancer Detection and Classification using Fusion of Squeeze-Excitation-Densenet with Metaheuristic-Driven Ensemble Deep Learning Models," *Scientific Reports*, vol. 15, no. 1, pp. 1-23, 2025. [CrossRef] [Google Scholar] [Publisher Link]

[9] Umesh Kumar Lilhore et al., "A Precise Model for Skin Cancer Diagnosis using Hybrid U-Net and Improved MobileNet-V3 with Hyperparameters Optimization," *Scientific Reports*, vol. 14, no. 1, pp. 1-24, 2024. [CrossRef] [Google Scholar] [Publisher Link]

[10] K.M. Monica et al., "Melanoma Skin Cancer Detection using Mask-RCNN with Modified GRU Model," *Frontiers in Physiology*, vol. 14, pp. 1-12, 2024. [CrossRef] [Google Scholar] [Publisher Link]

[11] Ishak Pacal, Melek Alaftekin, and Ferhat Devrim Zengul, "Enhancing Skin Cancer Diagnosis using Swin Transformer with Hybrid Shifted Window-based Multi-Head Self-Attention and SwiGLU-based MLP," *Journal of Imaging Informatics in Medicine*, vol. 37, no. 6, pp. 3174-3192, 2024. [CrossRef] [Google Scholar] [Publisher Link]

[12] Abayomi Bello, Sin-Chun Ng, and Man-Fai Leung, "Skin Cancer Classification using Fine-Tuned Transfer Learning of DENSENET-121," *Applied Sciences*, vol. 14, no. 17, pp. 1-25, 2024. [CrossRef] [Google Scholar] [Publisher Link]

[13] Mohamed Hosny et al., "Attention-based Convolutional Neural Network Model for Skin Cancer Classification," *IEEE Access*, vol. 13, pp. 172027-172050, 2025. [CrossRef] [Google Scholar] [Publisher Link]

[14] Rodrigue Bogne Tchema, Anastasis C. Polycarpou, and Marios Nestoros, "Skin Cancer Classification using Machine Learning," *Multimedia Tools and Applications*, vol. 84, no. 6, pp. 3239-325, 2025. [CrossRef] [Publisher Link]

[15] Vasuja Devi Midasala et al., "MFEUsLNet: Skin Cancer Detection and Classification using Integrated AI with Multilevel Feature Extraction-based Unsupervised Learning," *Engineering Science and Technology, an International Journal*, vol. 51, pp. 1-17, 2024. [CrossRef] [Google Scholar] [Publisher Link]

[16] Burhanettin Ozdemir, and Ishak Pacal, "A Robust Deep Learning Framework for Multiclass Skin Cancer Classification," *Scientific Reports*, vol. 15, no. 1, pp. 1-19, 2025. [CrossRef] [Google Scholar] [Publisher Link]

[17] Rizwan Ali et al., "A Novel SpaSA-based Hyperparameter-Optimized FCEDN with Adaptive CNN Classification for Skin Cancer Detection," *Scientific Reports*, vol. 14, no. 1, pp. 1-17, 2024. [CrossRef] [Google Scholar] [Publisher Link]

[18] Hugo Vega-Huerta et al., "Classification Model of Skin Cancer using Convolutional Neural Network," *Information Systems Engineering*, vol. 30, no. 2, pp. 387-394, 2025. [CrossRef] [Google Scholar] [Publisher Link]

[19] Ahmet Nusret Toprak, and Ibrahim Aruk, "A Hybrid Convolutional Neural Network Model for the Classification of Multi-Class Skin Cancer," *International Journal of Imaging Systems and Technology*, vol. 34, no. 5, pp. 1-18, 2024. [CrossRef] [Google Scholar] [Publisher Link]

[20] Fallah H. Najjar et al., "Transformer-Aided Skin Cancer Classification using VGG19-based Feature Encoding," *Scientific Reports*, vol. 15, no. 1, pp. 1-18, 2025. [CrossRef] [Google Scholar] [Publisher Link]

[21] Essam H. Houssein et al., "An Effective Multiclass Skin Cancer Classification Approach based on Deep Convolutional Neural Network," *Cluster Computing*, vol. 27, no. 9, pp. 12799-12819, 2024. [CrossRef] [Google Scholar] [Publisher Link]

[22] Zhanlin Ji et al., "EFAM-Net: A Multi-Class Skin Lesion Classification Model Utilizing Enhanced Feature Fusion and Attention Mechanisms," *IEEE Access*, vol. 12, pp. 143029-143041, 2024. [CrossRef] [Google Scholar] [Publisher Link]

[23] Yousef S. Alsahafi, Mohamed A. Kassem, and Khalid M. Hosny, "Skin-Net: A Novel Deep Residual Network for Skin Lesions Classification using Multilevel Feature Extraction and Cross-Channel Correlation with Detection of Outlier," *Journal of Big Data*, vol. 10, no. 1, pp. 1-23, 2023. [CrossRef] [Google Scholar] [Publisher Link]

[24] Sasmita Padhy et al., "Temporal Integration of ResNet Features with LSTM for Enhanced Skin Lesion Classification," *Results in Engineering*, vol. 25, pp. 1-13, 2025. [CrossRef] [Google Scholar] [Publisher Link]

[25] V.S.S. Bala Tripura Sathvika et al., "Pipelined Structure in the Classification of Skin Lesions based on AlexNet CNN and SVM Model with Bi-Sectional Texture Features," *IEEE Access*, vol. 12, pp. 57366-57380, 2024. [CrossRef] [Google Scholar] [Publisher Link]

[26] Sara Medhat et al., "Iterative Magnitude Pruning-based Light Version of AlexNet for Skin Cancer Classification," *Neural Computing and Applications*, vol. 36, no. 3, pp. 1413-1428, 2024. [CrossRef] [Google Scholar] [Publisher Link]

[27] Amany M. Sarhan et al., "Achieving High-Accuracy Skin Cancer Classification with Deep Learning Optimized by Ant Colony Algorithm," *Journal of Electrical Systems and Information Technology*, vol. 12, no. 1, pp. 1-25, 2025. [CrossRef] [Google Scholar] [Publisher Link]

[28] Omneya Attallah, "Skin Cancer Classification Leveraging Multi-Directional Compact Convolutional Neural Network Ensembles and Gabor Wavelets," *Scientific Reports*, vol. 14, no. 1, pp. 1-19, 2024. [CrossRef] [Google Scholar] [Publisher Link]

[29] Geunho Jung, Semin Kim, and Sangwook Yoo, "Skin Tone Analysis through Skin Tone Map Generation with Optical Approach and Deep Learning," *Skin Research and Technology*, vol. 30, no. 10, pp. 1-8, 2024. [CrossRef] [Google Scholar] [Publisher Link]

[30] K Scott Mader, Skin Cancer MNIST: HAM10000, 2018. [Online]. Available: https://www.kaggle.com/datasets/kmader/skin-cancer-mnist-ham10000

[31] Prasad Maharana, ISIC 2019 Skin Lesion images for classification, 2018. [Online]. Available: https://www.kaggle.com/datasets/salviohexia/isic-2019-skin-lesion-images-for-classification

[32] Sumaiya Binte Shahid, ISIC Challenge Dataset-2020, 2020. [Online]. Available: https://www.kaggle.com/datasets/sumaiyabinteshahid/isic-challenge-dataset-2020

[33] Mahdavi, Skin Cancer (PAD-UFES-20), 2020. [Online]. Available: https://www.kaggle.com/datasets/mahdavi1202/skin-cancer

[34] Nasraldeen Alnor Adam Khleel, and Károly Nehéz, "Software Defect Prediction using a Bidirectional LSTM Network Combined with Oversampling Techniques," *Cluster Computing*, vol. 27, no. 3, pp. 3615-3638, 2024. [CrossRef] [Google Scholar] [Publisher Link]

[35] D.R. Manjunath et al., "Predicting Diabetic Retinopathy and Nephropathy Complications using Machine Learning Techniques," *IEEE Access*, vol. 13, pp. 70228-70253, 2025. [CrossRef] [Google Scholar] [Publisher Link]

[36] Ahmed Hatem Soudy et al., "Deepfake Detection using Convolutional Vision Transformers and Convolutional Neural Networks," *Neural Computing and Applications*, vol. 36, no. 31, pp. 19759-19775, 2024. [CrossRef] [Google Scholar] [Publisher Link]